Journal of Statistical Mechanics:
Theory and Experiment

SISSA

PAPER: CLASSICAL STATISTICAL MECHANICS, EQUILIBRIUM AND NON-EQUILIBRIUM

The effect of side motion in the dynamics of interacting molecular motors

Journal of Statistical Mechanics: Theory and Experiment
An IOP and SISSA journal

PAPER: Classical statistical mechanics, equilibrium and non-equilibrium

The effect of side motion in the dynamics of interacting molecular motors

Tripti Midha[1], **Arvind Kumar Gupta**[1,3] **and Anatoly B Kolomeisky**[2]

[1] Department of Mathematics, Indian Institute of Technology Ropar, Rupnagar-140001, India
[2] Department of Chemistry and Center for Theoretical Biological Physics, Rice University, Houston, TX 77005, United States of America
E-mail: akgupta@iitrpr.ac.in

Received 3 March 2017
Accepted for publication 30 May 2017
Published 12 July 2017

Online at stacks.iop.org/JSTAT/2017/073202
https://doi.org/10.1088/1742-5468/aa75e1

Abstract. To mimic the collective motion of interacting molecular motors, we propose and discuss an open two-lane symmetrically coupled interactive TASEP model that incorporates interaction in the thermodynamically consistent fashion. We study the effect of both repulsive and attractive interaction on the system's dynamical properties using various cluster mean field analysis and extensive Monte Carlo simulations. The interactions bring correlations into the system, which were found to be reduced due to the side motion of particles. We produce the steady-state phase diagrams for symmetrically split interaction strength. The behavior of the maximal particle current with respect to the interaction energy E is analyzed for different coupling rates and interaction splittings. The results suggest that for strong coupling and large splittings, the maximal flow of the motors occurs at a weak attractive interaction strength which matches with the known experimental results on kinesin motor protein.

Keywords: driven diffusive systems, exclusion processes, molecular motors, stochastic particle dynamics

[3] Author to whom any correspondence should be addressed.

1742-5468/17/073202+24$33.00

Contents

1. Introduction

Molecular motors or motor proteins are the nanomachines that play a crucial role in all vital functions of a cell such as cell division, cell locomotion, cell motility, cargo transport along the filaments, etc [1–6]. During intracellular transport, they function in a team and drive the cargo transport along linear cytoskeletal filaments by transforming chemical energy, typically derived from ATP hydrolysis, into the mechanical energy [6]. Moreover, external energy suppliers can also support motor proteins' movement by generating electro-potential gradient [4, 5]. Uncovering the mechanisms of motor proteins has been a subject of multiple studies. In the last two decades, various single-molecular studies, *in vivo* and *in vitro* experiments as well as theoretical approaches, have sufficiently probed the mechanochemical and dynamic properties of motor proteins [4, 5, 7]. These single molecular level studies assure that the mechanism of molecular motors can not be fully explained without taking into account the reversibility of associated biochemical processes according to the fundamental laws of physics. Although these studies have provided a good insight over the properties of motor proteins, the collective behavior of motor proteins, which generally work in a team, needs yet to be well explored [5, 7, 8].

The recent experiments on microtubule-bound kinesin motor proteins indicate that they interact with their neighbors with some energy estimated to be weakly attractive ($1.6 \pm 0.5 k_{\mathrm{B}}T$) [9, 10]. The similar interactions can also be assumed to exist among other motor proteins. Such mutually attractive interactions might modify the coordination mechanism of motor proteins as well as the various chemical transitions such as hydrolysis of ATP, association and dissociation of motor protein from the track etc occurring at the single molecular level highlighting the important role of interactions on motor proteins' dynamics [5]. The multi-particle dynamics on non-equilibrium systems in physics, chemistry as well as in biology can be well replicated by the minimal model

J. Stat. Mech. (2017) 073202

among the class of driven diffusive system, totally asymmetric simple exclusion process (TASEP) [11–14]. Several variants of open and closed TASEP's have been utilized to analyze the collective dynamics of interacting molecular motors [15–20], but these studies were phenomenological and did not take into account the effect of interactions on microscopic level properties of motor proteins.

Recently, the coordination among interacting molecular motors has been analyzed using a new variant of open one-lane TASEP [21, 26] that can completely describe the effect of interactions on the chemical transitions occurring at the single molecular level. The theoretical approaches in these studies suggested the important role of correlations in the system. The optimal interaction strength for the maximal flow of the motors was found to be weakly repulsive which is in opposite regime of the interaction strength known through experiments [9]. Since the biochemical network of motor proteins includes multiple pathways which give the possibility for the motors to change lane. The mechanism of motor proteins can be well understood if the interactions' effect is observed on the various biochemical transitions of the motor proteins when they are moving collectively along the parallel cytoskeletal filaments [5].

In this paper, we consider the symmetric coupling in between two open parallel interacting TASEP lanes. The model can successfully capture the effect of inter as well as intra-lane interactions on the cooperative dynamics of motor proteins along linear filaments using fundamental thermodynamic way. We analyze the role of interactions and different coupling strengths on the steady-state phase diagrams, maximal particle current and correlations in the system using the various vertical cluster mean field theories and Monte Carlo simulations. Most importantly, we observe the effect of side motion and symmetry of interactions on the optimal interaction strength corresponding to the maximal current and relate the results with existing experimental predictions.

The paper is organized as follows. In section 2, we define our model and its governing dynamical rules. In sections 3.1 and 3.2, the non-equilibrium steady state (NESS) properties of the system are analyzed using different vertical cluster mean field theories. In section 4, we discuss the important results and analyze the role of side motion on cooperative mechanisms of interacting molecular motors. We also compare our theoretical results with Monte Carlo simulations, experimental evidence, and 1-lane interacting TASEP's results. We finally conclude in section 5.

2. Model description

To mimic the transport of motor proteins along parallel filaments, we define our model by considering an open two-lane coupled lattice comprising of $N \times 2$ sites, where N denotes the number of sites in each lane. Particles drift unidirectionally from the leftmost site of a lane to its rightmost site. Both first and last sites of each lane are connected with infinite reservoirs of particles. Particles obey the hard-core exclusion principle that says no two particles can simultaneously occupy the same site (figure 1). Each sth site ($1 \leqslant s \leqslant N$) of a tth lane ($t \in \{1, 2\}$) is assigned an occupation variable $\tau_{s,t} \in \{0, 1\}$, where $\tau_{s,t} = 1$ ($\tau_{s,t} = 0$) denotes the occupied (empty) state of the site.

https://doi.org/10.1088/1742-5468/aa75e1

J. Stat. Mech. (2017) 073202

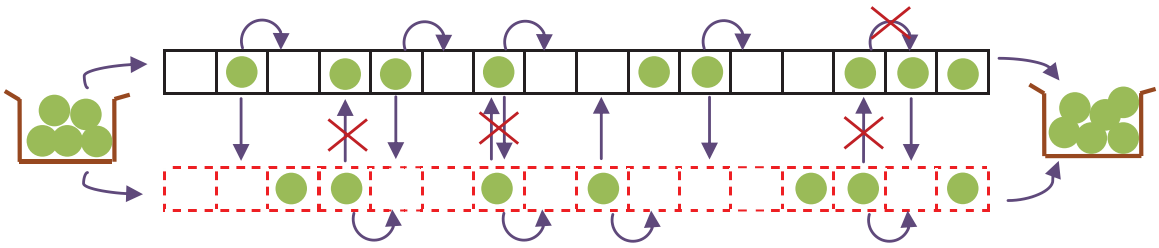

Figure 1. Schematic view of an open two-lane symmetrically coupled interacting TASEP model. Solid (black) and dotted (red) lattice represent lane 1 and lane 2, respectively. A filled circle denotes an occupied site whereas the absence of circle means an empty site. Arrows represent possible hoppings of the particles, whereas the crossed arrows mean there is no hopping.

Moreover, the nearest neighbor interaction of particles within the lane (intra-lane) and among particles of opposite lanes (inter-lane) are considered. It is assumed that an energy E is associated with a bond holding two particles together and the intra-lane hopping rates depend on whether the bond is broken or created [21]. We represent the rates associated with creating and breaking of pair of bonds by q and r, respectively. The intra-lane interactions are completely thermodynamically consistent. In the inter-lane interactions, a particle at an sth site of one lane can hop to its vertically opposite site, provided it is empty. Let ω $(0 \leqslant \omega \leqslant 1)$ be the rate associated with a vertical transition without taking into account the intra-channel interactions. Based on the breaking and making of horizontal bonds, the vertical transitions can occur from sixteen different configurations. Considering all the vertical transition rates namely six ω, four ωr, four ωq, one ωr^2 and one ωq^2 arising from the sixteen different configurations make the system dynamics quite complex. For simplicity, we assume the constant hopping rate ω which is dominating among all possible vertical rates. It can be thought of as the mean field approximation for all the configurations. Most importantly, in the case of lane changing of a particle with a rate ω, the horizontal transition rates in our model are modified keeping in view the fundamental thermodynamic concepts. However, it is assumed that the presence of the particle at the vertically opposite site of an sth site does not alter the intra-lane interactions. This approximation can be justified as there is no experimental evidence at present for such interactions of the particles in opposite lanes. The above considered dependency of the intra-lane interactions on the inter-lane transitions are not only limited to the case of motion of molecular motors but also applies to other transport processes such as vehicular traffic [22–25].

According to the random-sequential update rules, a site (s, t) is randomly selected from a randomly chosen lane t. To understand all possible hoppings arising from intra as well as inter-lane interactions, it is assumed that there is a particle at the (s, t)th site and the next site, $(s + 1,\ t)$th, is empty. For the case, when the latter site is occupied, the particle can hop to (s, t')th site (where $t' \neq t$), if it is empty, with a rate ω. At any infinitesimal small time step, a particle chosen for hopping is either isolated or a part of a cluster (non-isolated). Here, an isolated particle at the sth site means that its both leftmost and rightmost neighboring sites are vacant. Thus, whenever a particle shifts between its isolated and non-isolated states, the energy of the system and hence the hopping rates of the particle change. The dynamical rules in the bulk as shown in figure 2 (bulk rules) can be understood as follows. When $\tau_{s,t'} = 1(0)$, an isolated particle

J. Stat. Mech. (2017) 073202

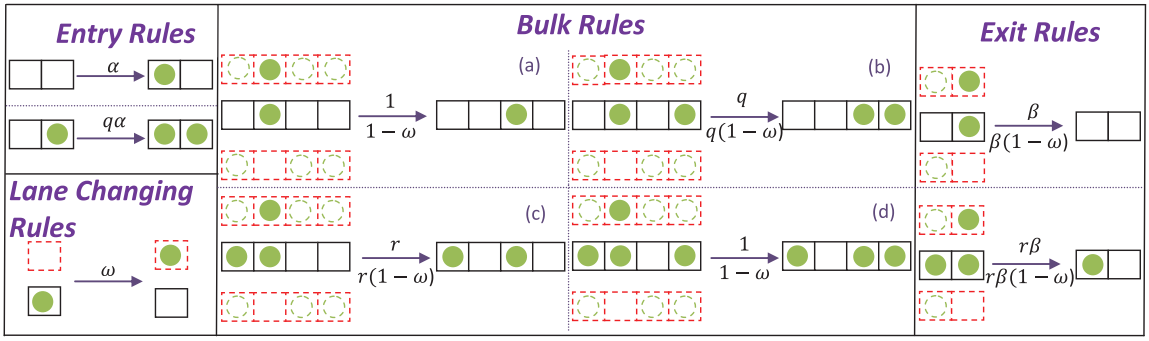

Figure 2. The solid (black) and the dotted (red) lattice, respectively, reflect a portion of lane 1 and lane 2. The dotted open circles depict that the site can either be empty or occupied. The filled circles and the empty sites, respectively, indicate the presence and absence of particles. The transition rules for different possible hoppings in lane 1 given the configuration of lane 2 are shown and their corresponding rates are mentioned above and below the arrows.

at the (s,t)th site hops to the next site with a rate q ($q(1-\omega)$) to become non-isolated and with a rate 1 ($1-\omega$), to become isolated. Whereas, a non-isolated particle at the (s,t)th site breaks its bond to become either isolated with a rate r ($r(1-\omega)$) or non-isolated with a rate 1 ($1-\omega$) at the next site, when the vertically opposite site, (s,t') th, is occupied (empty). Further, if any horizontal hopping does not takes place the particle at (s,t)th site can shift to the vertically opposite empty site with a rate ω (figure 2-Lane changing rules).

The effect of interactions have also been incorporated at the boundaries (figure 2—entry and exit rules). A particle can enter from the left reservoir to an empty first site of a lane, to become either isolated with a rate α or non-isolated with a rate $q\alpha$. Whereas, a non-isolated particle at Lth site leaves with a rate $r\beta$ in the presence of the particle at the opposite site, otherwise in the absence the rate is $r\beta(1-\omega)$. In the case of an isolated particle at Lth site, the exit rate is β when the vertically opposite site is occupied, otherwise the hopping rate is $\beta(1-\omega)$. If the particle does not leave, it can shift its lane with a rate ω when $\tau_{L,t'}=0$.

The hopping rates associated with the shifting from isolated to non-isolated state and vice-versa can be understood in terms of opposing chemical transition that leads to the relation $\frac{q}{r}=\mathrm{e}^{\frac{E}{k_\mathrm{B}T}}$ [26]. Here, $k_\mathrm{B}T$ represents the thermodynamic energy, where k_B and T are respectively, the Boltzmann constant and thermodynamic temperature. To manage the effect of interaction energy E on stepping rates q and r, a dimensionless splitting parameter θ ($0\leqslant\theta\leqslant 1$) is introduced which explicitly determines q and r as

$$q=\mathrm{e}^{\frac{\theta E}{k_\mathrm{B}T}},\qquad r=\mathrm{e}^{\frac{(\theta-1)E}{k_\mathrm{B}T}}. \tag{1}$$

Here, the rates q and r vary according to the strength of interaction energy E. For the case of attractive interaction ($E>0$), the bond making rate, q, is larger as comparative to bond breaking rate, r. However, the reverse happens for repulsive interactions ($E<0$). For the special case, $E=0$, the model reduces to the original two-lane symmetrically coupled TASEP model [22]. When the interactions are repulsive, system's dynamics can also represent vehicular traffic flow, where a vehicle generally moves at a

J. Stat. Mech. (2017) 073202

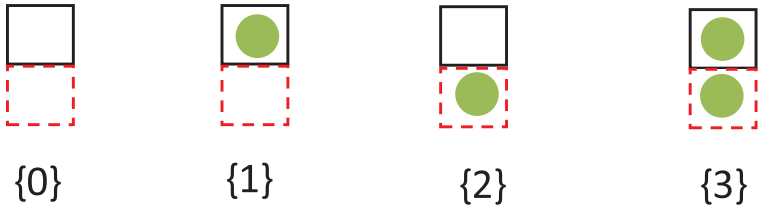

Figure 3. Four possible states of a 1-vertical cluster in a two-lane system.

higher rate ($r > 1$) if it is followed behind by an another vehicle. However, it generally slows down its speed ($q < 1$) when a vehicle finds another vehicle in its following path [23].

3. Cluster mean field theory

Mean field analysis has worked as an important tool to explore the qualitative properties of interacting many-body systems. The simple mean field theory that neglects all correlations between the state variables works well for a system with zero or very weak interactions [24, 27]. Systems in which, a particle's dynamics depend strongly upon its neighboring sites can be analyzed more appropriately using cluster mean field analysis that considers some correlation between the state variables [28–33]. A general n-cluster mean field approximation treats a cluster of n neighboring sites exactly. Here, any large cluster of size (say) $k \geqslant n$ is factorized into the product of clusters of n sites with two neighboring clusters having $(n-1)$ common sites. The inter-lane interactions in a two-lane system can be analyzed by treating a (1-) vertical cluster made up of two vertically opposite sites exactly. Let us denote a 1-vertical cluster consisting of sth site of both the lanes by $\xi_s = \tau_{s,t}\tau_{s,t'}$, where $t \neq t' \in \{1, 2\}$. Based on the occupancy of the sth site of both the lanes, ξ_s can exist in one of the four possible states namely $\{0\}$, $\{1\}$, $\{2\}$, and, $\{3\}$. When both sites of ξ_s are occupied (empty), its state is $\{3\}$ ($\{0\}$). Whereas, ξ_s is in state $\{1\}$ or $\{2\}$, depending on the occupied state of lane 1 or lane 2, respectively (figure 3). Let V_i denote the probability of a 1-vertical cluster to be in state $\{i\}$, where $i \in \{0, 1, 2, 3\}$. Now, we define a n-vertical cluster to be a cluster consisting of n successive 1-vertical clusters. According to the system's dynamics, the particle current in each lane is affected by the inter as well as intra-channel interactions and can be analyzed for any site in the bulk by considering a 4-vertical cluster (figure 2—bulk rules). Let V_{ijkl} denote the probability of a 4-vertical cluster in state $\{ijkl\}$, where $\{i\}, \{j\}, \{k\}$ and $\{l\}$, respectively, denote the states of first, second, third and fourth 1-vertical cluster. Considering all the eight possible hoppings as shown in configurations figures 2(a)–(d), the total bulk current for lane 1 can be expressed as

$$J_{\text{bulk}} = \sum_{j=\{1,3\}} \sum_{k=\{0,2\}} \left(1 - \frac{(3-j)}{2}\omega\right) \left[\sum_{i=\{0,2\}} \left(\sum_{l=\{0,2\}} V_{ijkl} + q \sum_{l=\{1,3\}} V_{ijkl} \right) + \sum_{i=\{1,3\}} \left(r \sum_{l=\{0,2\}} V_{ijkl} + \sum_{l=\{1,3\}} V_{ijkl} \right) \right]. \tag{2}$$

J. Stat. Mech. (2017) 073202

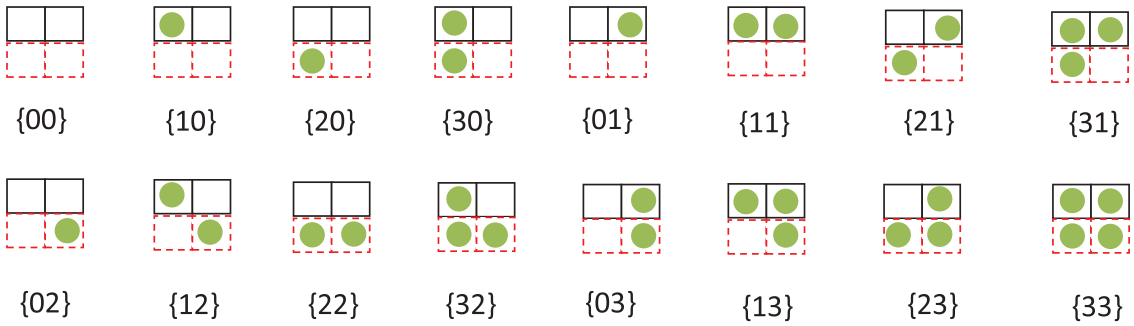

Figure 4. Sixteen possible states of a 2-vertical cluster in a two-lane system.

Similarly a particle's entry and exit dynamics can be analyzed using a 2-vertical cluster (figure 2). Based on the states of first and second vertical cluster, (say) $\{i\}$ and $\{j\}$, respectively, a 2-vertical cluster can be found in sixteen different states denoted by $\{ij\}$, where $i, j \in \{0, 1, 2, 3\}$ (see figure 4). Let V_{ij} denote the probability of a 2-vertical cluster in state $\{ij\}$, then the particle current at the entry and exit sites for lane 1 can be written as

$$J_{\text{entr}} = \alpha \sum_{i,j=\{0,2\}} V_{ij} + q\alpha \sum_{\substack{i=\{0,2\} \\ j=\{1,3\}}} V_{ij}, \tag{3}$$

$$J_{\text{exit}} = \beta \sum_{j=\{1,3\}} \left[\left(1 - \frac{(3-j)}{2}\omega \right) [(V_{0j} + V_{2j}) + r(V_{1j} + V_{3j})] \right]. \tag{4}$$

One can obtain the similar expression of the particle current at the bulk and the boundaries for lane 2. Now, we determine the characteristics of the system by simplifying the current expressions using cluster mean field analysis.

3.1. 1-vertical cluster mean field theory (1-VCMFT)

The 1-vertical cluster mean field theory [22] treats a vertical cluster exactly but completely ignores the correlations between two neighboring vertical clusters. The mutually exclusive and exhaustive nature of the four states of a 1-vertical cluster implies

$$\sum_{i=0}^{3} V_i = 1. \tag{5}$$

The probability of a 4-vertical cluster and 2-vertical cluster, under the 1-VCMFT approach, can be factorised as

$$V_{ijkl} \approx V_i V_j V_k V_l, \tag{6}$$

$$V_{ij} \approx V_i V_j.$$

Thus, the bulk current and the boundary currents expressions from equations (2)–(4) simplifies to

$$J_{\text{bulk}} = (V_3 + (1-\omega)V_1)(1-\rho_1)[(2-q-r)(\rho_1^2 - \rho_1) + 1], \tag{7}$$

J. Stat. Mech. (2017) 073202

$$J_{\text{entr}} = \alpha(1-\rho_1)(1-\rho_1+q\rho_1), \tag{8}$$

$$J_{\text{exit}} = \beta((1-\omega)V_1+V_3)(1-\rho_1+r\rho_1).$$

Here, $\rho_1 = V_1 + V_3$ is the density of lane 1. The particle current from the above equations can be determined if the probability of each 1-vertical cluster is known. The master equations for V_i's, under the 1-VCMFT approach, can be written as

$$\frac{\mathrm{d}V_0}{\mathrm{d}t} = \sum_{i=1}^{2}\Big[[V_0((1-\omega)V_i+V_3)-(1-\omega)V_i(1-\rho_i)] \times [(2-q-r)(\rho_i^2-\rho_i)+1]\Big], \tag{9}$$

$$\begin{aligned}\frac{\mathrm{d}V_1}{\mathrm{d}t} &= [V_0((1-\omega)V_1+V_3)-(1-\omega)V_1(1-\rho_1)] \\ &\times [(2-q-r)(\rho_1^2-\rho_1)+1] \\ &+ [V_3(V_0+V_1)-V_1((1-\omega)V_2+V_3)] \\ &\times [(2-q-r)(\rho_2^2-\rho_2)+1]+\omega(V_2-V_1),\end{aligned} \tag{10}$$

$$\begin{aligned}\frac{\mathrm{d}V_2}{\mathrm{d}t} &= [V_0((1-\omega)V_2+V_3)-(1-\omega)V_2(1-\rho_2)] \\ &\times [(2-q-r)(\rho_2^2-\rho_2)+1] \\ &+ [V_3(V_0+V_2)-V_2((1-\omega)V_1+V_3)] \\ &\times [(2-q-r)(\rho_1^2-\rho_1)+1]+\omega(V_1-V_2),\end{aligned} \tag{11}$$

$$\frac{\mathrm{d}V_3}{\mathrm{d}t} = \sum_{\substack{j=1\\ j\neq i}}^{2}\sum_{i=1}^{2}\Big[V_j((1-\omega)V_i+V_3)-V_3(1-\rho_i)\Big] \times [(2-q-r)(\rho_i^2-\rho_i)+1]. \tag{12}$$

Here, $\rho_2 = V_2 + V_3$ is the density for lane 2. The above master equations at steady state reduces to

$$V_3V_0 = (1-\omega)V_1V_2, \tag{13}$$

$$\text{and} \qquad V_1 = V_2.$$

It is noteworthy to mention that equation (13) is free from intra-lane interaction parameters q and r and thus, it match exactly with the steady state conditions of the two channel symmetrically coupled TASEP model without interactions [22]. Additionally, it implies that $\rho_1 = \rho_2 = \rho$ and combining it with the normalization condition, we get

$$V_1 = \begin{cases}\frac{-V_3+\sqrt{V_3^2+(1-\omega)V_3(1-V_3)}}{1-\omega}, & \omega \neq 1\\ \frac{1-V_3}{2}, & \omega = 1.\end{cases} \tag{14}$$

Now, the particle current can explicitly be expressed as a function of single-ordered parameter, V_3, which for $\omega \neq 1$ implies

J. Stat. Mech. (2017) 073202

$$J_{\text{bulk}} = \frac{c(1-c-\omega(1-V_3))}{(1-\omega)^3}\Big[(1-\omega)^2 + (2-q-r) \times (\omega(1+\omega)V_3^2 + (1-\omega(\omega-2c))V_3 - c(1-\omega))\Big], \tag{15}$$

$$J_{\text{entr}} = \frac{\alpha(1-c-\omega(1-V_3))}{(1-\omega)^2}\Big[1-c(1+q)-\omega(1-(1+q)V_3)\Big], \tag{16}$$

$$J_{\text{exit}} = \frac{\beta c}{(1-\omega)}\Big[1-c(1-r)-\omega(1-(1-r)V_3)\Big]. \tag{17}$$

Here, $c = \sqrt{V_3(1-\omega(1-V_3))}$.

For the case of strong coupling ($\omega = 1$), the particle current can be computed separately as the system has only 2 types of vertical clusters: fully filled and half filled. The non-existence of fully empty vertical cluster leads to zero particle current for a non-zero entrance rate, that is physically irrelevant [22]. Thus, the particle currents per channel are simplified to

$$J_{\text{bulk}} = \frac{V_3(1-V_3)}{8}\Big[(q+r)(1-V_3^2) + 2(1+V_3^2)\Big], \tag{18}$$

$$J_{\text{entr}} = \frac{\alpha(1-V_3)}{4}\Big[(1-V_3) + q(1+V_3)\Big], \tag{19}$$

$$J_{\text{exit}} = \frac{\beta V_3}{2}\Big[(1-V_3) + r(1+V_3)\Big]. \tag{20}$$

Alternatively, the above expressions of particle currents, for $\omega = 1$, can also be obtained by mapping the proposed system into an effective single channel interacting TASEP system. The fully filled vertical clusters can be interpreted as particles, whereas the half-filled vertical clusters with the particle only at the upper and the lower site are, respectively, interpreted as holes of type A_1 and A_2. Then, the particle current and density per channel of the proposed system is related to the particle current, J^*, and density, $\rho^* = V_3$, of the effective one-channel system by the following relations:

$$J = \frac{J^*}{2}, \ \rho = \frac{(1+\rho^*)}{2}.$$

Note that if there is no interaction i.e. $E = 0$, then A_1 and A_2 are identical, and the system is mapped into original single-channel TASEP model with entrance rate as α and exit rate as 2β.

Next, we derive the steady-state phase diagrams for intermediate as well as for strong coupling. When the bulk current dominates and remains unaffected by the entrance and exit rates, the system attains the maximal current (MC) phase. In this phase, the condition $\frac{\partial J_{\text{bulk}}}{\partial V_3} = 0$ holds, which for $\omega \neq 1$ implies

J. Stat. Mech. (2017) 073202

$$
\begin{aligned}
&c(1-\omega)^2(2-q-r)(1-c-\omega(1-V_3))\\
&\times\Big[1-2c-2\omega(1-4V_3+2cV_3)+\omega^2(8V_3^2-4V_3(c+2)+2c+1)\Big]\\
&+\Big[(1-\omega)^2+(2-q-r)\Big(\omega(1+\omega)V_3^2+(1-\omega^2-2c\omega)V_3-c(1-\omega)\Big)\Big]\\
&\times\Big[2c^2(1-\omega(1-2V_3)-2c\omega)-(1-\omega(1-2V_3)(1-c-\omega(1-V_3)))\Big]=0,
\end{aligned}
\tag{21}
$$

and for $\omega = 1$ yields

$$
(2+q+r)(1-2V_3)+(2-q-r)V_3^2(3-4V_3)=0. \tag{22}
$$

The above equations can be solved for relevant root, V_3^{MC} which eventually provides V_1^{MC}, density, ρ_{MC} and maximal current, J_{MC}.

For the low density (LD) phase, entrance current dominates the bulk dynamics. Thus, the continuity of current implies $J_{\mathrm{entr}} = J_{\mathrm{bulk}}$ which gives

$$
\alpha=\begin{cases}\frac{(V_3+(1-\omega)V_1)(1-(2-q-r)\rho(1-\rho))}{(1+(q-1)\rho)}, & \omega\neq 1\\ \frac{V_3((q+r)(1-V_3^2)+2(1+V_3^2))}{2(1-V_3+q(1+V_3))}, & \omega=1.\end{cases} \tag{23}
$$

The above equations can be utilized to calculate the relevant root, $V_3^{\mathrm{LD}}(\alpha)$, which further gives V_1^{LD}, the density, ρ_{LD} and the particle current in the LD phase. The second-order continuous phase transition line between LD and MC phases can be found by substituting V_1 and V_3 from MC phase in the above equations.

For the case when exit current limits the bulk dynamics, the system attains the high density (HD) phase. V_3^{HD}, the density, ρ_{HD} and the particle current can be obtained using equation of continuity for the exit and bulk current that gives

$$
\beta=\begin{cases}\frac{(1-\rho)(1-(2-q-r)\rho(1-\rho))}{(1+(r-1)\rho)}, & \omega\neq 1\\ \frac{(1-V_3)((q+r)(1-V_3^2)+2(1+V_3^2))}{4(1-V_3+q(1+V_3))}, & \omega=1.\end{cases} \tag{24}
$$

Additionally, the second-order continuous phase transition line between the HD and MC phases can be obtained from the above relations by substituting $V_3 = V_3^{\mathrm{MC}}$ and $\rho = \rho_{\mathrm{MC}}$ from the MC phase.

The first order continuous phase transition line between LD and HD phases can be constructed from the condition, $J_{\mathrm{entr}} = J_{\mathrm{exit}}$, which gives the following relation between α and β:

$$
\alpha=\begin{cases}\frac{\beta(1+(r-1)\rho_{\mathrm{HD}})(V_3^{\mathrm{LD}}+(1-\omega)V_1^{\mathrm{LD}})}{(1-\rho_{\mathrm{HD}})(1+(q-1)\rho_{\mathrm{LD}})}, & \omega\neq 1\\ \frac{2\beta V_3^{\mathrm{LD}}(1-V_3^{\mathrm{HD}}+r(1+V_3^{\mathrm{HD}}))}{(1-V_3^{\mathrm{HD}})(1-V_3^{\mathrm{LD}}+q(1+V_3^{\mathrm{LD}}))}, & \omega=1.\end{cases} \tag{25}
$$

3.2. 2-vertical cluster mean field theory (2-VCMFT)

In contrast to the 1-VCMFT, the 2-vertical cluster mean field theory (2-VCMFT) considers the correlation and treats two neighboring vertical clusters exactly. The mutually exclusive and collectively exhaustive nature of 2-vertical cluster's probabilities imply

J. Stat. Mech. (2017) 073202

$$\sum_{i=0}^{3}\sum_{j=0}^{3} V_{ij} = 1. \tag{26}$$

The definition of density together with the relation $V_1 = V_2$ under the Kolmogorov consistency conditions for the given translational invariant system imply

$$\sum_{i=\{1,3\}}\sum_{j=0}^{3} V_{ij} = \sum_{i=\{1,3\}}\sum_{j=0}^{3} V_{ji} = \sum_{i=\{2,3\}}\sum_{j=0}^{3} V_{ij} = \sum_{i=\{2,3\}}\sum_{j=0}^{3} V_{ji} = \rho. \tag{27}$$

Clearly,

$$V_i = \sum_{j=0}^{3} V_{ij} \qquad \text{and} \tag{28}$$

$$\sum_{j=0}^{3} V_{ij} = \sum_{j=0}^{3} V_{ji}, \qquad \text{for } i \in \{0,1,2,3\}. \tag{29}$$

The probability of a 4-vertical cluster, V_{ijkl}, under 2-VCMFT approximation, can be written as

$$V_{ijkl} = V_{i|\underline{j}} V_{jk} V_{\underline{k}|l}, \tag{30}$$

where,

$$V_{i|\underline{j}} = \frac{V_{ij}}{\sum_{i=0}^{3} V_{ij}}, \quad V_{\underline{k}|l} = \frac{V_{kl}}{\sum_{l=0}^{3} V_{kl}}. \tag{31}$$

Thus, the bulk current expression from equation (2) simplifies to

$$J_{\text{bulk}} = \sum_{j=\{1,3\}}\sum_{k=\{0,2\}} \left(1 - \frac{(3-j)}{2}\omega\right)\left(\frac{V_{jk}}{V_j V_k}\right)\left[\sum_{i=\{0,2\}}\left(\sum_{l=\{0,2\}} V_{ij}V_{kl} + q\sum_{l=\{1,3\}} V_{ij}V_{kl}\right)\right.$$
$$\left. + \sum_{i=\{1,3\}}\left(r\sum_{l=\{0,2\}} V_{ij}V_{kl} + \sum_{l=\{1,3\}} V_{ij}V_{kl}\right)\right]. \tag{32}$$

Note that the entrance and exit current from equations (3) and (4) remain intact under 2-VCMFT approximation as they are already in terms of 2-vertical cluster probabilities. Now, the dynamical properties of the system such as density, particle current can be obtained if all the 2-vertical cluster probabilities are known. Since there are sixteen unknown probabilities; it requires sixteen independent equations to find V_{ij}'s. The master equation for V_{33}, in terms of 4-vertical cluster probabilities, gives

J. Stat. Mech. (2017) 073202

$$\begin{aligned}\frac{\mathrm{d}V_{33}}{\mathrm{d}t} &= q(1-\omega)[V_{0213}+V_{1213}+V_{0123}+V_{2123}]\\ &+ q[V_{0313}+V_{1313}+V_{0323}+V_{2323}]\\ &+ (1-\omega)[V_{2213}+V_{3213}+V_{1123}+V_{3123}]\\ &+ [V_{2313}+V_{3313}+V_{1323}+V_{3323}]\\ &- r[2V_{3300}+V_{3320}+V_{3302}+V_{3322}+V_{3310}+V_{3301}+V_{3311}]\\ &- [V_{3301}+V_{3302}+V_{3321}+V_{3312}+V_{3323}+V_{3313}+2V_{3303}],\end{aligned} \tag{33}$$

which, under 2-VCMFT approximation, in steady state reduces to

$$\begin{aligned}&\sum_{\substack{i=1\\ i\neq k}}^{3}\sum_{\substack{j=1\\ j\neq k}}^{2}\sum_{k=1}^{2}\left(1-\frac{(3-i)}{k}\omega\right)\frac{V_{ik}V_{k3}}{V_iV_k}[(V_{ji}+V_{3i})+q(V_{0i}+V_{ki})]\\ &=\sum_{\substack{i=0\\ i\neq k}}^{2}\sum_{\substack{j=1\\ j\neq k}}^{2}\sum_{k=1}^{2}\frac{V_{33}V_{3i}}{V_3V_i}\left[(V_{ik}+V_{i3})+r(V_{i0}+V_{ij})\right].\end{aligned} \tag{34}$$

Similarly, the master equations for other fifteen 2-vertical cluster probabilities can be obtained (see appendix). Now, in totality, we have twenty-five equations among which a system of sixteen independent equations can be chosen appropriately. One set of sixteen independent equations is equations (26), (27) and ((29) for $i=3$), (A.1)–(A.3), (A.5)–(A.9), (A.11) and (A.15). Although such highly non-linear system of equations can not be solved analytically, their numerical solution can be obtained as a function of parameter ρ.

We now derive the steady-state phase diagrams of the interactive system using current expressions obtained under 2-VCMFT analysis. For each value of q and r, there corresponds a density, ρ_{MC} (say) at which J_{bulk} is maximum and the system attains the maximal current phase. For $\rho > \rho_{\mathrm{MC}}$, the bulk current is found to be equal to the exit current and the system reaches the exit dominated phase or high density phase. Similarly, for $\rho < \rho_{\mathrm{MC}}$, the system enters into low density (LD) phase, and it gives the bulk current to be same as the entrance current. As entrance rate limits the bulk current, the phase is also said to be an entrance dominated phase.

The two-phase coexistence lines can be computed in a similar fashion as obtained for the 1-VCMFT approach. The second order continuous phase transition line separating LD (HD) and MC phase is obtained by equating the particle current as well as density of both the phases. Similarly, the first order continuous LD–HD phase boundary line is obtained by equating the entrance and exit current.

4. Results and discussion

In this section, we discuss the effect of different attractive and repulsive interaction strength as well as various coupling rates on boundary induced phase transitions, maximal particle current and correlations in the system using approximation theories discussed in the previous section. To find the best-suited theory for the interactive

J. Stat. Mech. (2017) 073202

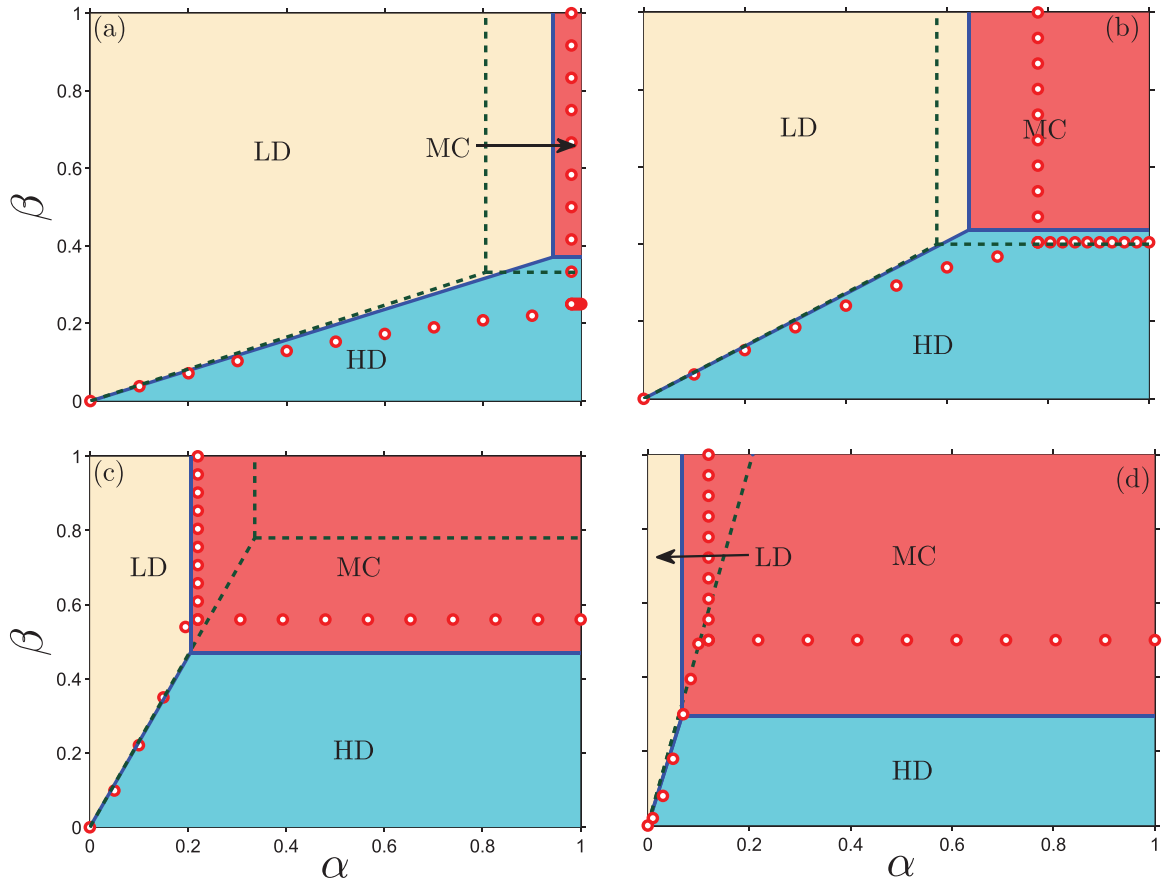

Figure 5. Stationary phase diagrams for interactive two-channel symmetrically coupled TASEP with coupling strength $\omega = 0.2$ and splitting parameter $\theta = 0.5$ for : (a) $E = -1.7k_BT$; (b) $E = -0.7k_BT$; (c) $E = 1.6k_BT$; (d) $E = 3k_BT$. Solid lines, dotted lines and markers, respectively represent the results of the 2-VCMFT, 1-VCMFT and simulations.

system, we compared the results with extensive Monte Carlo simulations (MCS). We considered the system of 2000 lattice sites to avoid any finite size and boundary effects and adopted a random-sequential update algorithm. Each simulation was run over 10^9–10^{10} time steps and first 20% of time steps were avoided to reach steady state. While computing the phase boundary lines, the density profiles and particle current were compared with a precision of 0.01.

Firstly, we would like to point out that in the absence of interactions both theoretical approaches namely the 1-VCMFT and 2-VCMFT yield the same results which match exactly with the simulation results. Now, for a fixed coupling strength, we analyze the effect of attractive as well as repulsive interactions on the phase diagram (figure 5). As compared to simulations, for repulsive and weakly attractive interactions the 1-VCMFT approach works reasonably well but fails to predict the MC phase in the $[0, 1] \times [0, 1]$ phase plane of (α, β) for the case of stronger attractive interactions (see figure 5(d)). Whereas, the 2-VCMFT results are in good agreement with simulations for both types of interactions. Parallel to the case of single channel interactive TASEP [26], it is found that the interactions do not alter the topology of the phase diagram of a two-channel symmetrically coupled system. However, the quantitative changes

J. Stat. Mech. (2017) 073202

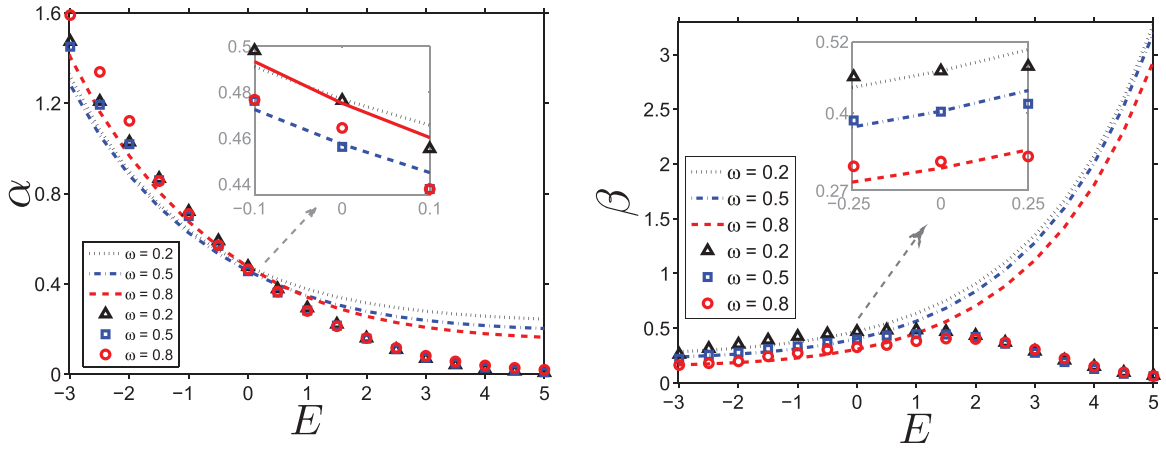

Figure 6. Coordinates of the triple points in the phase diagram as a function of the interaction energy, E in terms of k_BT under different coupling rates. Different lines and markers, respectively represent the results of the 1-VCMFT and 2-VCMFT. The inset figures show the zoomed results of $E = 0$. Simulation results match qualitatively with 2-VCMFT results and have not been shown to avoid overlapping.

i.e. shifting in the location of triple points and phase transition lines are observed. In the case of repulsive interactions, the LD–HD and HD–MC phase transition lines shift downwards, while the LD–MC line moves rightwards which results in the enlargement of the LD region (figures 5(a) and (b)). The reason for the observed behavior is that repulsive interaction decreases the effective entrance rate ($q < 1$) and increases the effective exit rate ($r > 1$). However, the opposite happens in the case of attractive interactions where the effective entrance rate increases ($q > 1$) and the effective exit rate decreases ($r < 1$). As a result, the LD region shrinks and the HD, MC phases dominate the phase diagram (figures 5(c) and (d)).

We now analyze the effect of side motion on the interactive TASEP's phase diagram by plotting the coordinates of the triple point for various interaction energy (figure 6). It is clear from figure 6 that the nature of α and β coordinates with respect to the interaction energy remains qualitatively the same under all coupling strengths. As interaction energy increases from repulsive to attractive, the 2-VCMFT approach complemented with simulations indicate that the α coordinate decreases monotonically and tends towards zero, thus implying the disappearance of LD region. Whereas, under the 1-VCMFT analysis, the qualitative nature of the α coordinate remains same but saturates to a non-zero value (figure 6(a)). The β coordinate of the triple points obtained from the 1-VCMFT analysis increases monotonically with respect to interaction energy, while its behavior is non-monotonous under 2-VCMFT analysis and simulations. One can conclude that the 1-VCMFT completely fails for large attractions as, here, the β coordinate increases without bound (figure 6(b)). Now, we observe the effect of ω on the behavior of α and β coordinates under the 1-VCMFT and 2-VCMFT analysis for different interaction strength. For the case of repulsive and weakly attractive interactions, both the theories predict that the β coordinate decreases monotonically, whereas the α coordinate shows non-monotonous behavior on increasing the coupling rate. The similar behavior of α and β coordinates was observed in the case of

J. Stat. Mech. (2017) 073202

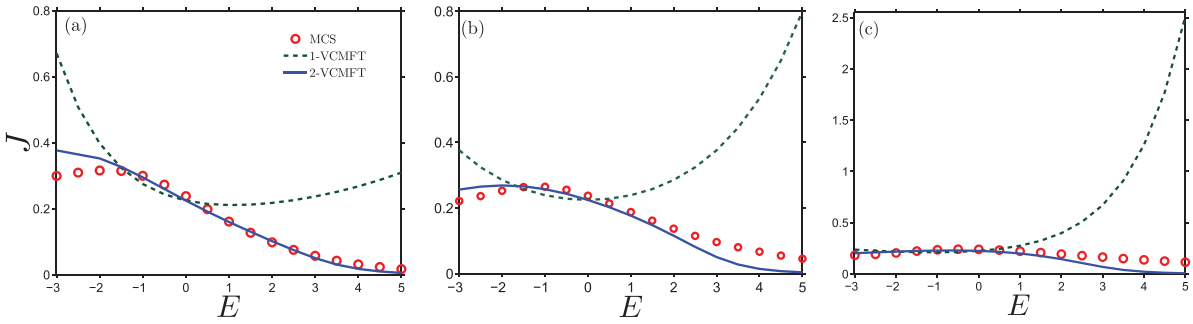

Figure 7. The maximal particle current as a function of interaction energy, E in terms of k_BT, under the coupling strength $\omega = 0.2$ for : (a) $\theta = 0.25$; (b) $\theta = 0.5$; (c) $\theta = 0.75$.

no interactions [22]. Under the strong attractive interactions, the 2-VCMFT shows an increase in both the α and β coordinates while the 1-VCMFT predicts decreasing trend in both the coordinates with increment in the coupling strength (figure 6).

To further understand the role of interactions in our system, we plot the maximal particle current with respect to interaction energy for different energy splittings (figure 7). The maximal particle current predicted by the 1-VCMFT matches with simulation results for weak interactions and completely disagrees for large interactions, where it predicts the particle current to increase without bound (figure 7). This is physically irrelevant because in the presence of large attractive interactions, particles form a big cluster which obstructs their movement and makes current to approach towards zero. While in the case of strong repulsions, a particle may not have any neighbor, and in this situation, the system can behave like TASEP with dimers whose current saturates and thus, can not increase without bound [22, 34]. On the other hand, the maximal particle current computed from the 2-VCMFT approach agrees well with the simulations for all range of interactions. The maximal particle current is found to be a unimodal function of the interaction energy E, whose maximum value occurs at a weak repulsive interaction strength (figure 7). This indicates that interactions in a coupled TASEP system can maximize the flow of particles. These results are important for the kinesin motor proteins from the experimental point of view. It is known that kinesin motor proteins form patches during their movement along the cytoskeletal filaments [10]. Such attractive interaction within the motors is found to be of order $E = (1.6 \pm 0.5)k_BT$, which is important for the robust functioning of the motor proteins [9]. The theoretical methods namely a cluster mean field, and the modified cluster mean field for the one channel system reported that optimal interaction strength corresponding to the maximal current occurs for repulsive interactions [21, 26]. These theoretical results are in opposite regime to the experimental results on kinesin motor protein [9]. As their model was limited to one channel and neglected many realistic features of motor proteins such as lane changing, backwards stepping, etc the results can not be generalized. Our proposed system includes the effect of side motion of particles as well as energy splittings, it will be interesting to observe their effect on the optimal interaction strength, E^* that corresponds to the maximal current. Figure 8 shows the theoretical results of the optimal interaction strength corresponding to the maximal particle current with respect to the coupling rate ω for different energy splittings. It is found that for most of the interaction splittings (except $\theta \approx 1$), the optimal interaction strength belongs to the

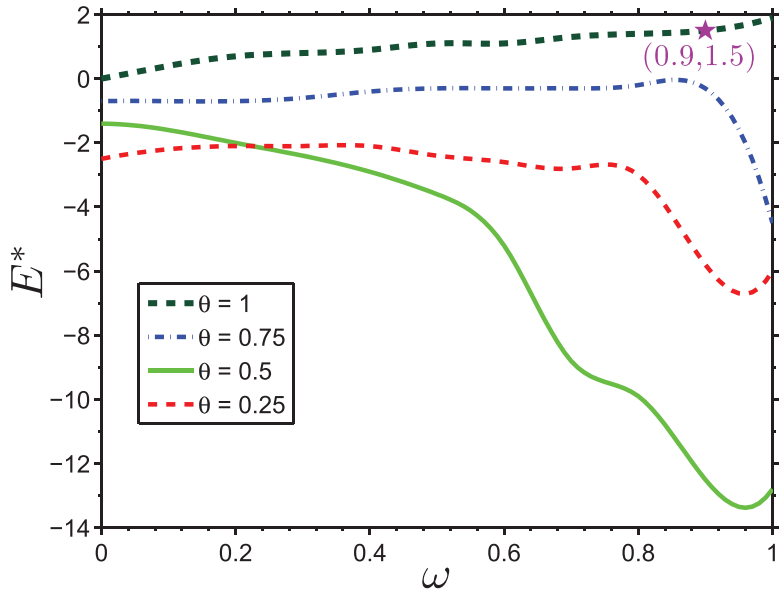

Figure 8. The effect of coupling rate (ω) on the optimal interaction strength (E^*) for different interaction splittings predicted using 2-VCMFT.

case of repulsive interaction irrespective of coupling rate. However, when formation of the particle cluster is much affected by the interactions (i.e. $\theta \approx 1$), the optimal interaction strength for maximal particle current is achieved at weakly attractive strength for all values of coupling rates. Moreover, when $\theta = 1$ and $\omega \approx 0.9$, the maximal particle current is optimized at the interaction strength known through experiments (figure 9). This shows the importance of coupling on kinesin motor proteins that they can maximize their flow while functioning vigorously [9, 10]. The knowledge of how frequently the real motor proteins change lanes and how the interaction effects their movement can not be predicted from our mesoscopic theoretical method. Their determination will require the more advanced experimental and theoretical approaches.

Our theoretical analysis and simulations show that in an interactive system, spatial correlation plays an important role. We now explore the correlations in our system using cluster mean field analysis and validate the results with extensive Monte Carlo simulations. Since the correlations are uniform in the bulk, we define a correlation function C between two neighboring vertical clusters (say) ξ_s and ξ_{s+1} as

$$C = \langle \xi_s \xi_{s+1} \rangle - \langle \xi_s \rangle \langle \xi_{s+1} \rangle, \tag{35}$$

where $s = 1, 2, \cdots, N-1$. $\langle \cdots \rangle$ denotes the expected value, which for a 1-vertical cluster gives

$$\langle \xi_s \rangle = \langle \tau_{s,t} \tau_{s,t'} \rangle = \sum_{\tau_{s,t}} \sum_{\tau_{s,t'}} \tau_{s,t} \tau_{s,t'} P(\tau_{s,t}, \tau_{s,t'}) = V_3. \tag{36}$$

Here, $P(\tau_{s,t}, \tau_{s,t'})$ denotes the probability of the sth vertical cluster, ξ_s. The above expectation is non-zero only when the sth site of both the lanes is occupied. The expectation of two neighboring vertical cluster is given by

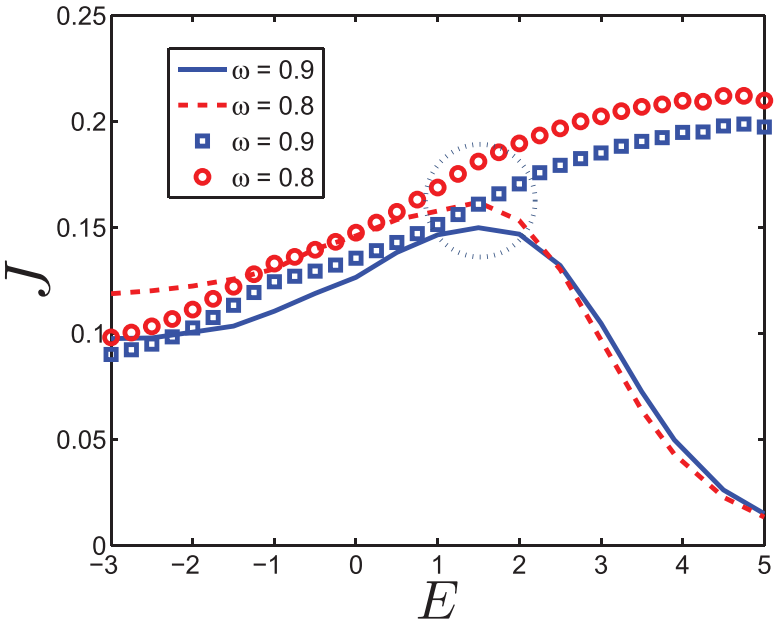

Figure 9. The maximal particle current as a function of interaction energy E for $\theta = 1$ and $\omega = 0.8, 0.9$. Lines and markers, respectively represent the results of 2-VCMFT and simulations.

$$\langle \xi_s \xi_{s+1} \rangle = \langle \tau_{s,t} \tau_{s,t'} \tau_{s+1,t} \tau_{s+1,t'} \rangle$$
$$= \sum_{\tau_{s,t}} \sum_{\tau_{s,t'}} \sum_{\tau_{s+1,t}} \sum_{\tau_{s+1,t'}} \tau_{s,t} \tau_{s,t'} \tau_{s+1,t} \tau_{s+1,t'} P(\tau_{s,t}, \tau_{s,t'}, \tau_{s+1,t}, \tau_{s+1,t'}). \quad (37)$$

Here, $P(\tau_{s,t}, \tau_{s,t'}, \tau_{s+1,t}, \tau_{s+1,m'})$ represents the joint probability of two neighboring vertical cluster whose state depends upon the occupancy state of the four sites involved in the 2-vertical cluster. If all the four sites are occupied then the above expression is non-zero and is given by V_{33}.

We plot the correlation curves computed theoretically and through simulations for different interaction splittings (figure 10). Under the 1-VCMFT analysis, the function C predicts zero correlation, which is in accordance with the fact that the theory completely ignores the connection between two neighboring state variables. The correlation curves predicted from the 2-VCMFT approach are in good agreement with the simulation results for repulsive and weakly attractive interactions, whereas they match qualitatively for stronger attractive interactions. The 2-VCMFT results complemented with simulations clearly justify the physical meaning of the correlation function which represents the scope of $(s+1)$th vertical cluster to fully occupy in the case of fully occupied sth vertical cluster. For the case of repulsion, the presence of particles at one vertical cluster does not allow its neighboring vertical cluster to occupy. In this situation, the two clusters are negatively correlated and we get $C < 0$. When the interactions are attractive, the particles at one vertical cluster attract other particles to their neighboring vertical cluster. In this situation, the vertical clusters are positively correlated which gives $C > 0$. At $E = 0$, the hopping rates of particles become independent of the neighboring sites, hence both the theories and simulations imply zero correlation in the system. On comparing our results with one lane, it is observed that the effect of

J. Stat. Mech. (2017) 073202

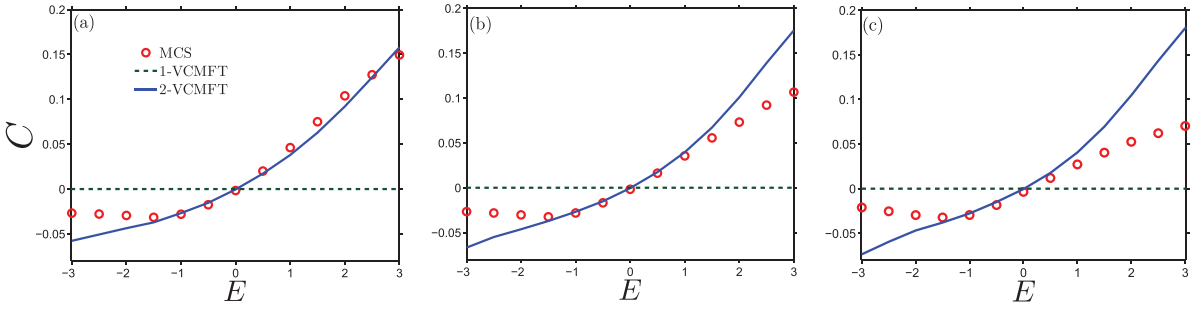

Figure 10. Correlation curves as a function of interaction energy, E in terms of k_BT, under the coupling rate $\omega = 0.2$ for : (a) $\theta = 0.25$; (b) $\theta = 0.5$; (c) $\theta = 0.75$. In simulations, $\alpha = 1$, $\beta = 1$ is utilized.

lane changing of particles considerably reduces the magnitude of the correlation function [26].

Now, we justify the reason for why the 2-VCMFT worked well in capturing the correlations for repulsive and weaker attractive but not for stronger attractive interactions. In the case of repulsion, for a particle at the sth site, the probability of finding a particle at the $(s+1)$th site is less and for the subsequent sites is much less. It indicates that the correlations decay very fast and are *short-range* which can be managed by the 2-VCMFT. On the contrary, for the attractive interactions, the situation is quite opposite since the presence of a particle at the sth site increases the probability of having a particle at the $(s+1)$th as well as at the further sites. Thus the expected correlations are *long-range* and strong which can not be sufficiently captured by the 2-VCMFT[4]. Hence it can be inferred that if n-vertical cluster ($n > 2$) mean field theory is utilized, then all correlations in the system can be apprehended.

5. Conclusion

In this work, we have discussed a variant of two-lane symmetrically coupled TASEP model in which the transition rules are modified to incorporate the nearest neighbor interactions via short range energy E in a thermodynamically consistent fashion. We analyzed the model using two theoretical methods namely the 1-VCMFT that captures the inter-lane interactions but ignores the intra-lane interactions, and the 2-VCMFT that can study inter as well as intra-lane interactions. The theoretical methods along with extensive Monte Carlo simulations can analytically or numerically calculate the effect of side motion of particles as well as the nearest-neighbor interactions on the steady-state phase diagrams, the location of triple points and the maximal particle current. The results suggest an important role of correlations in the system. The 1-VCMFT approach that can analytically calculate the current expressions and phase diagrams works well for weak interactions and completely fails for large interactions. The 2-VCMFT approach was successful in capturing the *short-range* correlations and matched qualitatively with simulations for all range of interactions. It was found

[4] Similar seemingly surprising differences have been observed when interacting driven diffusive systems were first studied, with theoretical understanding being well-established subsequently [35]

J. Stat. Mech. (2017) 073202

that the side motion of particles reduces the correlations in the system. We also analyzed the effect of symmetry of interactions and side motion of particles on the optimal interaction strength. It was observed that when the formation of cluster is strongly influenced and breaking of cluster is weakly influenced by interactions, the optimal interaction strength, E^* is achieved at a weak attractive strength under the strong coupling. We also discussed the importance of these results for kinesin motor proteins and found them to be in agreement with the known experimental results.

Acknowledgments

AK Gupta gratefully acknowledges the financial support from Department of Science and Technology (DST) (Grant No. SB/FTP/MS-001/2013), Government of India.

Appendix. Master equations for 2-vertical cluster probabilities

In this appendix, we represent other 15 equations in steady state. From $\frac{dV_{32}}{dt} = 0$, we have

$$\begin{aligned}
&\sum_{\substack{i=1\\ i\neq k}}^{3}\sum_{\substack{j=1\\ j\neq k}}^{2}\sum_{k=1}^{2}\left[\left(1-\frac{(3-i)}{k}\omega\right)\frac{V_{ik}V_{k2}}{V_iV_k}[C_k(V_{0i}+V_{ki})+D_k(V_{ji}+V_{3i})]\right]+\omega(V_{31}-V_{32})\\
&\quad+\sum_{i=0}^{2}\left[\frac{V_{33}V_{3i}}{V_3V_i}[(V_{i1}+V_{i3})+r(V_{i0}+V_{i2})]\right]\\
&\quad=(1-\omega)\sum_{i=0}^{1}\left[\frac{V_{32}V_{2i}}{V_2V_i}[(V_{i2}+V_{i3})+r(V_{i0}+V_{i1})]\right]\\
&\quad+\sum_{i=0}^{1}\left[\frac{V_{32}}{V_3V_2}\Big(V_{i3}+V_{(i+2)3}\Big)[A_i(V_{21}+V_{23})+B_i(V_{20}+V_{22})]\right] \qquad \text{(A.1)}
\end{aligned}$$

From $\frac{dV_{31}}{dt} = 0$, we have

$$\begin{aligned}
&\sum_{\substack{i=1\\ i\neq k}}^{3}\sum_{\substack{j=1\\ j\neq k}}^{2}\sum_{k=1}^{2}\left[\left(1-\frac{(3-i)}{k}\omega\right)\frac{V_{ik}V_{k1}}{V_iV_k}[C_j(V_{0i}+V_{ki})+D_j(V_{ji}+V_{3i})]\right]+\omega(V_{32}-V_{31})\\
&\quad+\sum_{i=0}^{1}\left[\frac{V_{33}V_{3i}}{V_3V_i}[r(V_{i0}+V_{i1})+(V_{i2}+V_{i3})]\right]\\
&\quad=(1-\omega)\sum_{j=\{0,2\}}\left[\frac{V_{31}V_{1j}}{V_1V_j}[(V_{j1}+V_{j3})+r(V_{j0}+V_{j2})]\right]\\
&\quad+\frac{V_{31}}{V_3V_1}\sum_{i=\{0,2\}}\left[\Big(V_{i3}+V_{(i+1)3}\Big)\Big[A_i(V_{12}+V_{13})+B_i(V_{10}+V_{11})\Big]\right] \qquad \text{(A.2)}
\end{aligned}$$

From $\frac{\mathrm{d}V_{30}}{\mathrm{d}t}=0$, we have

$$\sum_{\substack{i=1\\ i\neq k}}^{3}\sum_{\substack{j=1\\ j\neq k}}^{2}\sum_{k=1}^{2}\left[\left(1-\frac{(3-i)}{k}\omega\right)\frac{V_{ik}V_{k0}}{V_iV_k}[(V_{0i}+V_{ki})+r(V_{ji}+V_{3i})]\right]$$
$$+\sum_{\substack{i=0\\ i\neq k}}^{2}\sum_{\substack{j=1\\ j\neq k}}^{2}\sum_{k=1}^{2}\left[(1-\omega)\frac{V_{3k}V_{ki}}{V_kV_i}[(V_{ik}+V_{i3})+r(V_{i0}+V_{ij})]\right]$$
$$=\sum_{\substack{i=0\\ i\neq k}}^{2}\sum_{\substack{j=1\\ j\neq k}}^{2}\sum_{k=1}^{2}\left[\frac{V_{30}}{V_3V_0}\left(V_{i3}+V_{(i+k)3}\right)\left[A_i(V_{0j}+V_{03})+B_i(V_{00}+V_{0k})\right]\right] \tag{A.3}$$

From $\frac{\mathrm{d}V_{23}}{\mathrm{d}t}=0$, we have

$$\sum_{i=0}^{1}\left[\frac{V_{32}}{V_3V_2}\Big(V_{i3}+V_{(i+2)3}\Big)\Big[A_i(V_{21}+V_{23})+B_i(V_{20}+V_{22})\Big]\right]+\omega(V_{13}-V_{23})$$
$$+\sum_{i=\{2,3\}}\left[\Big(1-(3-i)\omega\Big)\frac{V_{i0}V_{03}}{V_iV_0}\Big[(V_{2i}+V_{3i})+q(V_{0i}+V_{1i})\Big]\right]$$
$$=\sum_{\substack{i=0\\ i\neq k}}^{2}\sum_{\substack{j=1\\ j\neq k}}^{2}\sum_{k=1}^{2}\left[\frac{V_{23}V_{3i}}{V_3V_i}\left[C_k(V_{ik}+V_{i3})+D_k(V_{i0}+V_{ij})\right]\right]$$
$$+\sum_{i=\{1,3\}}\left[\Big(1-\frac{(3-i)}{2}\omega\Big)\frac{V_{i2}V_{23}}{V_iV_2}\Big[(V_{1i}+V_{3i})+q(V_{0i}+V_{2i})\Big]\right] \tag{A.4}$$

From $\frac{\mathrm{d}V_{22}}{\mathrm{d}t}=0$, we have

$$\sum_{i=\{2,3\}}\left[\Big(1-(3-i)\omega\Big)\frac{V_{i0}V_{02}}{V_iV_0}\Big[(V_{2i}+V_{3i})+q(V_{0i}+V_{1i})\Big]\right]$$
$$+\sum_{i=\{0,2\}}\left[\frac{V_{23}V_{3i}}{V_3V_i}\Big[(V_{i0}+V_{i2})+q(V_{i1}+V_{i3})\Big]\right]$$
$$=\sum_{i=\{1,3\}}\left[\Big(1-\frac{(3-i)}{2}\omega\Big)\frac{V_{i2}V_{22}}{V_iV_2}\Big[(V_{0i}+V_{2i})+r(V_{1i}+V_{3i})\Big]\right]$$
$$+(1-\omega)\sum_{i=\{0,1\}}\left[\frac{V_{22}V_{2i}}{V_2V_i}\Big[(V_{i2}+V_{i3})+r(V_{i0}+V_{i1})\Big]\right]+\omega(2V_{22}-V_{12}-V_{21}) \tag{A.5}$$

From $\frac{\mathrm{d}V_{21}}{\mathrm{d}t}=0$, we have

$$\sum_{i=0}^{1}\left[\frac{V_{30}}{V_3V_0}\Big(V_{i3}+V_{(i+2)3}\Big)\Big[A_i(V_{01}+V_{03})+B_i(V_{00}+V_{02})\Big]\right]+\omega(V_{11}+V_{22}-2V_{21})$$
$$+\sum_{i=\{2,3\}}\left[\Big(1-(3-i)\omega\Big)\frac{V_{i0}V_{01}}{V_iV_0}\Big[(V_{0i}+V_{1i})+r(V_{2i}+V_{3i})\Big]\right]$$
$$+\sum_{i=\{0,1\}}\left[\frac{V_{23}V_{3i}}{V_3V_i}\Big[(V_{i2}+V_{i3})+r(V_{i0}+V_{i1})\Big]\right]$$
$$=(1-\omega)\left[\frac{V_{21}}{V_2V_1}\sum_{i=\{0,2\}}\left[\Big(V_{i2}+V_{(i+1)2}\Big)\Big[A_i(V_{12}+V_{13})+B_i(V_{10}+V_{11})\Big]\right]\right.$$
$$\left.+\sum_{i=\{0,2\}}\left[\frac{V_{21}V_{1i}}{V_1V_i}[(V_{i0}+V_{i2})+q(V_{i1}+V_{i3})]\right]\right]$$
$$+\sum_{i=\{1,3\}}\left[\Big(1-\frac{(3-i)}{2}\omega\Big)\frac{V_{i2}V_{21}}{V_iV_2}\Big[(V_{1i}+V_{3i})+q(V_{0i}+V_{2i})\Big]\right] \tag{A.6}$$

From $\frac{\mathrm{d}V_{20}}{\mathrm{d}t}=0$, we have

$$\sum_{i=\{2,3\}}\left[\Big(1-(3-i)\omega\Big)\frac{V_{i0}V_{00}}{V_iV_0}\Big[(V_{0i}+V_{1i})+r(V_{2i}+V_{3i})\Big]\right]+\omega(V_{10}-V_{20})$$
$$+(1-\omega)\sum_{\substack{i=0\\i\neq k}}^{2}\sum_{\substack{j=1\\j\neq k}}^{2}\sum_{k=1}^{2}\left[\frac{V_{2k}V_{ki}}{V_kV_i}[C_k(V_{ik}+V_{i3})+D_k(V_{i0}+V_{ij})]\right]$$
$$=(1-\omega)\frac{V_{20}}{V_2V_0}\sum_{i=\{0,2\}}\left[\Big(V_{i2}+V_{(i+1)2}\Big)\Big[A_i(V_{02}+V_{03})+B_i(V_{00}+V_{01})\Big]\right]$$
$$+\sum_{i=\{1,3\}}\left[\Big(1-\frac{(3-i)}{2}\omega\Big)\frac{V_{i2}V_{20}}{V_iV_2}\Big[(V_{0i}+V_{2i})+r(V_{1i}+V_{3i})\Big]\right] \tag{A.7}$$

From $\frac{\mathrm{d}V_{13}}{\mathrm{d}t}=0$, we have

$$\sum_{i=\{1,3\}}\left[\Big(1-\frac{(3-i)}{2}\omega\Big)\frac{V_{i0}V_{03}}{V_iV_0}\Big[(V_{1i}+V_{3i})+q(V_{0i}+V_{2i})\Big]\right]+\omega(V_{23}-V_{13})$$
$$+\frac{V_{31}}{V_3V_1}\sum_{i=\{0,2\}}\Big[(V_{i3}+V_{(i+1)3})[A_i(V_{12}+V_{13})+B_i(V_{10}+V_{11})]\Big]$$
$$=\sum_{i=\{0,1\}}\left[\frac{V_{13}V_{3i}}{V_3V_i}[(V_{i0}+V_{i1})+q(V_{i2}+V_{i3})]\right]+\sum_{i=\{0,2\}}\left[\frac{V_{13}V_{3i}}{V_3V_i}[(V_{i1}+V_{i3})+r(V_{i0}+V_{i2})]\right]$$
$$+\sum_{i=\{2,3\}}\left[\Big(1-(3-i)\omega\Big)\frac{V_{i1}V_{13}}{V_iV_1}\Big[(V_{2i}+V_{3i})+q(V_{0i}+V_{1i})\Big]\right] \tag{A.8}$$

J. Stat. Mech. (2017) 073202

From $\frac{dV_{12}}{dt} = 0$, we have

$$\frac{V_{30}}{V_3V_0}\sum_{i=\{0,2\}}\left[\Big(V_{i3}+V_{(i+1)3}\Big)\Big[A_i(V_{02}+V_{03})+B_i(V_{00}+V_{01})\Big]\right]+\omega(V_{11}+V_{22}-2V_{12})$$
$$+\sum_{i=\{1,3\}}\left[\Big(1-\frac{(3-i)}{2}\omega\Big)\frac{V_{i0}V_{02}}{V_iV_0}\Big[(V_{0i}+V_{2i})+r(V_{1i}+V_{3i})\Big]\right]$$
$$+\sum_{i=\{0,2\}}\left[\frac{V_{13}V_{3i}}{V_3V_i}\Big[(V_{i1}+V_{i3})+r(V_{i0}+V_{i2})\Big]\right.$$
$$=(1-\omega)\left[\sum_{i=\{0,1\}}\left[\frac{V_{12}V_{2i}}{V_2V_i}\Big[(V_{i0}+V_{i1})+q(V_{i2}+V_{i3})\Big]\right]\right]$$
$$+\sum_{i=\{2,3\}}\left[\Big(1-(3-i)\omega\Big)\frac{V_{i1}V_{12}}{V_iV_1}\Big[(V_{2i}+V_{3i})+q(V_{0i}+V_{1i})\Big]\right]$$
$$+(1-\omega)\frac{V_{12}}{V_1V_2}\sum_{i=\{0,1\}}\left[(V_{i1}+V_{(i+2)1})[A_i(V_{21}+V_{23})+B_i(V_{20}+V_{22})]\right]\Bigg] \tag{A.9}$$

From $\frac{dV_{11}}{dt} = 0$, we have

$$\sum_{i=\{1,3\}}\left[\Big(1-\frac{(3-i)}{2}\omega\Big)\frac{V_{i0}V_{01}}{V_iV_0}[(V_{1i}+V_{3i})+q(V_{0i}+V_{2i})]\right]$$
$$+\sum_{i=\{0,1\}}\left[\frac{V_{13}V_{3i}}{V_3V_i}[(V_{i0}+V_{i1})+q(V_{i2}+V_{i3})]\right]$$
$$+\sum_{i=\{2,3\}}\left[\Big(1-(3-i)\omega\Big)\frac{V_{i1}V_{11}}{V_iV_1}\Big[(V_{0i}+V_{1i})+r(V_{2i}+V_{3i})\Big]\right]+\omega(2V_{11}-(V_{12}+V_{21}))$$
$$=(1-\omega)\sum_{i=\{0,2\}}\left[\frac{V_{11}V_{1i}}{V_1V_i}[(V_{i1}+V_{i3})+r(V_{i0}+V_{i2})]\right] \tag{A.10}$$

From $\frac{dV_{10}}{dt} = 0$, we have

$$\sum_{i=\{1,3\}}\left[\Big(1-\frac{(3-i)}{2}\omega\Big)\frac{V_{i0}V_{00}}{V_iV_0}\Big[(V_{0i}+V_{2i})+r(V_{1i}+V_{3i})\Big]\right]+\omega(V_{20}-V_{10})$$
$$+(1-\omega)\sum_{\substack{i=0\\i\neq j}}^{2}\sum_{\substack{j=1\\j\neq k}}^{2}\sum_{k=1}^{2}\left[\frac{V_{1j}V_{ji}}{V_jV_i}[C_k(V_{ij}+V_{i3})+D_k(V_{i0}+V_{ik})]\right]$$
$$=(1-\omega)\frac{V_{10}}{V_1V_0}\sum_{i=\{0,1\}}\left[(V_{0i}+V_{0(i+2)})\Big[C_i(V_{01}+V_{21})+D_i(V_{11}+V_{31})\Big]\right]$$
$$+\sum_{i=\{2,3\}}\left[\Big(1-(3-i)\omega\Big)\frac{V_{i1}V_{10}}{V_iV_1}\Big[(V_{0i}+V_{1i})+r(V_{2i}+V_{3i})\Big]\right] \tag{A.11}$$

J. Stat. Mech. (2017) 073202

From $\frac{dV_{03}}{dt} = 0$, we have

$$
\begin{aligned}
&(1-\omega)\sum_{\substack{i=0\\ i\neq k}}^{2}\sum_{\substack{j=1\\ j\neq k}}^{2}\sum_{k=1}^{2}\left[\frac{V_{jk}}{V_jV_k}(V_{ij}+V_{(i+k)\,j})\Big[A_i(V_{kj}+V_{k3})+B_i(V_{k0}+V_{kk})\Big]\right]\\
&\quad=\sum_{\substack{i=0\\ i\neq k}}^{2}\sum_{\substack{j=1\\ j\neq k}}^{2}\sum_{k=1}^{2}\left[\frac{V_{03}V_{3i}}{V_3V_i}\left[(V_{i0}+V_{ij})+q(V_{ik}+V_{i3})\right]\right]\\
&\quad+(1-\omega)\sum_{\substack{j=1\\ j\neq k}}^{2}\sum_{k=1}^{2}\left[\frac{V_{k0}V_{03}}{V_kV_0}\left[(V_{kk}+V_{3k})+q(V_{0k}+V_{jk})\right]\right]\\
&\quad+\frac{V_{30}V_{03}}{V_3V_0}\Big((qV_{03}+V_{33})[(1+q)(V_{13}+V_{23})]\Big)
\end{aligned}
\tag{A.12}
$$

From $\frac{dV_{02}}{dt} = 0$, we have

$$
\begin{aligned}
&(1-\omega)\frac{V_{20}}{V_2V_0}\sum_{i=\{0,2\}}\left[\Big(V_{i2}+V_{(i+1)2}\Big)\Big[A_i(V_{02}+V_{03})+B_i(V_{00}+V_{01})\Big]\right]+\omega(V_{01}-V_{02})\\
&\quad+\sum_{i=\{0,2\}}\left[\frac{V_{03}V_{3i}}{V_3V_i}[(V_{i0}+V_{i2})+q(V_{i1}+V_{i3})]\right]\\
&\quad=(1-\omega)\sum_{i=\{0,1\}}\left[\frac{V_{02}V_{2i}}{V_2V_i}[(V_{i0}+V_{i1})+q(V_{i2}+V_{i3})]\right]\\
&\quad+\sum_{i=\{1,3\}}\left[\Big(1-\frac{(3-i)}{2}\omega\Big)\frac{V_{i0}V_{02}}{V_iV_0}\Big[(V_{0i}+V_{2i})+r(V_{1i}+V_{3i})\Big]\right]\\
&\quad+\sum_{i=\{2,3\}}\left[\Big(1-(3-i)\omega\Big)\frac{V_{i0}V_{02}}{V_iV_0}\Big[(V_{2i}+V_{3i})+q(V_{0i}+V_{1i})\Big]\right]
\end{aligned}
\tag{A.13}
$$

From $\frac{dV_{01}}{dt} = 0$, we have

$$
\begin{aligned}
&(1-\omega)\frac{V_{10}}{V_1V_0}\sum_{i=\{0,1\}}\left[(V_{i1}+V_{(i+2)1})[A_i(V_{01}+V_{03})+B_i(V_{00}+V_{02})]\right]+\omega(V_{02}-V_{01})\\
&\quad+\sum_{i=\{0,1\}}\left[\frac{V_{03}V_{3i}}{V_3V_i}\Big[(V_{i0}+V_{i1})+q(V_{i2}+V_{i3})\Big]\right]\\
&\quad=(1-\omega)\sum_{i=\{0,2\}}\left[\frac{V_{01}V_{1i}}{V_1V_i}\Big[(V_{i0}+V_{i2})+q(V_{i1}+V_{i3})\Big]\right]\\
&\quad+\sum_{i=\{1,3\}}\left[\Big(1-\frac{(3-i)}{2}\omega\Big)\frac{V_{i0}V_{01}}{V_iV_0}\Big[(V_{1i}+V_{3i})+q(V_{0i}+V_{2i})\Big]\right]\\
&\quad+\sum_{i=\{2,3\}}\left[\Big(1-(3-i)\omega\Big)\frac{V_{i0}V_{01}}{V_iV_0}\Big[(V_{0i}+V_{1i})+r(V_{2i}+V_{3i})\Big]\right]
\end{aligned}
\tag{A.14}
$$

J. Stat. Mech. (2017) 073202

From $\frac{dV_{00}}{dt} = 0$, we have

$$(1-\omega)\sum_{\substack{i=0\\ i\neq k}}^{2}\sum_{\substack{j=1\\ j\neq k}}^{2}\sum_{k=1}^{2}\left[\frac{V_{0k}V_{ki}}{V_kV_i}\left[(V_{i0}+V_{ij})+q(V_{ik}+V_{i3})\right]\right]$$
$$=\sum_{\substack{i=1\\ i\neq j}}^{3}\sum_{\substack{j=1\\ j\neq k}}^{2}\sum_{k=1}^{2}\left[\left(1-\frac{(3-i)}{j}\omega\right)\frac{V_{i0}V_{00}}{V_iV_0}\left[(V_{0i}+V_{ji})+r(V_{ki}+V_{3i})\right]\right] \quad \text{(A.15)}$$

Here, constants $(A_0, B_0) = (q, 1)$, $A_i = 1$, and $B_i = r$ for $i = \{1, 2\}$. $(C_0, D_0) = (1, r), (C_1, D_1) = (q, 1)$ and $(C_2, D_2) = (1, r)$.

References

[1] Howard J 2001 *Mechanics of Motor Proteins and the Cytoskeleton* (Sunderland, MA: Sinauer Associates)
[2] Bray D 2001 *Cell Movements: from Molecules to Motility* (New York: Garland)
[3] Kolomeisky A B and Fisher M E 2007 *Annu. Rev. Phys. Chem.* **58** 675–95
[4] Chowdhury D 2013 *Phys. Rep.* **529** 1–97
[5] Kolomeisky A B 2013 *J. Phys.: Condens. Matter* **25** 463101
[6] Kolomeisky A B 2015 *Motor Proteins and Molecular Motors* (Boca Raton, FL: CRC)
[7] Uppulury K, Efremov A K, Driver J W, Jamison D K, Diehl M R and Kolomeisky A B 2012 *J. Phys. Chem.* B **116** 8846–55
[8] Neri I, Kern N and Parmeggiani A 2013 *New J. Phys.* **15** 085005
[9] Roos W H *et al* 2008 *Phys. Biol.* **5** 046004
[10] Vilfan A, Frey E, Schwabl F, Thormählen M, Song Y H and Mandelkow E 2001 *J. Mol. Biol.* **312** 1011–26
[11] Kolomeisky A B, Schütz G M, Kolomeisky E B and Straley J P 1998 *J. Phys. A: Math. Gen.* **31** 6911
[12] MacDonald C T, Gibbs J H and Pipkin A C 1968 *Biopolymers* **6** 1–25
[13] Chou T, Mallick K and Zia R 2011 *Rep. Prog. Phys.* **74** 116601
[14] Parmeggiani A, Franosch T and Frey E 2003 *Phys. Rev. Lett.* **90** 086601
[15] Hager J, Krug J, Popkov V and Schütz G 2001 *Phys. Rev.* E **63** 056110
[16] Antal T and Schütz G 2000 *Phys. Rev.* E **62** 83
[17] Klumpp S and Lipowsky R 2004 *Europhys. Lett.* **66** 90
[18] Hao Q Y, Jiang R, Hu M B, Jia B and Wang W X 2016 *Sci. Rep.* **6** 19652
[19] Hao Q Y, Chen Z, Sun X Y, Liu B B and Wu C Y 2016 *Phys. Rev.* E **94** 022113
[20] Pinkoviezky I and Gov N S 2013 *New J. Phys.* **15** 025009
[21] Teimouri H, Kolomeisky A B and Mehrabiani K 2015 *J. Phys. A: Math. Theor.* **48** 065001
[22] Pronina E and Kolomeisky A B 2004 *J. Phys. A: Math. Gen.* **37** 9907
[23] Helbing D 2001 *Rev. Mod. Phys.* **73** 1067
[24] Derrida B 1998 *Phys. Rep.* **301** 65–83
[25] Appert-Rolland C, Ebbinghaus M and Santen L 2015 *Phys. Rep.* **593** 1–59
[26] Celis-Garza D, Teimouri H and Kolomeisky A B 2015 *J. Stat. Mech.* P04013
[27] Derrida B and Evans M R 1997 *Nonequilibrium Statistical Mechanics in One Dimension* (Cambridge: Cambridge University Press) pp 277–304
[28] Chowdhury D, Santen L and Schadschneider A 2000 *Phys. Rep.* **329** 199–329
[29] Schadschneider A and Schreckenberg M 1993 *J. Phys. A: Math. Gen.* **26** L679
[30] Schreckenberg M, Schadschneider A, Nagel K and Ito N 1995 *Phys. Rev.* **51** 2939
[31] Szabó G, Szolnoki A and Bodócs L 1991 *Phys. Rev.* A **44** 6375
[32] Szolnoki A and Szabó G 1993 *Phys. Rev.* E **48** 611
[33] Dickman R 1986 *Phys. Rev.* A **34** 4246
[34] Lakatos G and Chou T 2003 *J. Phys. A: Math. Gen.* **36** 2027
[35] Schmittmann B and Zia R K P 1995 *Phase Transitions and Critical Phenomena* vol 17 (London: Academic) pp 3–214

J. Stat. Mech. (2017) 073202